Eng. Sci., 2022, **20**, 341–351

Engineered Science

DOI: https://dx.doi.org/10.30919/es8d767

Nanoparticles and Bacterial Interaction of Host-Pathogens and the Detection Enhancement of Biomolecules by Fluorescence Raman Spectroscopic Investigation

G. Satpathy,[1, 2] G. K. Chandra,[3] K. Elayaraja,[4] D. R. Mahapatra,[2] A. Subramania,[5] Zhanhu Guo,[6,*] Siva Umapathy[7, 8] and E. Manikandan[9, 10,*]

Abstract

In this investigation, metal nanoparticles (NPs) have been used as antibiotics to inhibit the growth of bacteria. Here, we report an antibacterial study of ZnO-NPs, Co-NPs, and Au-NPs towards the approach to detecting the pathogenic strain of *Escherichia coli* (*E. coli)* cells. The nanoparticle (NP) acts as the detector probe for both live and dead pathogenic *E. coli* cells. The aim is to investigate the antibacterial bio-activities of metal NPs and their mode of action against pathogenic bacteria on the whole cell. Antibacterial activities of NPs were assessed by the agar diffusion method quantitatively, and the quality and quantity of *E. coli* cells extraction in the presence of nanoparticles (ZnO-NPs, Au-NPs, Co-NPs). The optimized concentration kills the pathogenic *E. coli* cells and hence shows the enrichment of cells. Results indicate that highly efficient nanoparticles inhibit the growth of such pathogenic microorganisms. Nanoparticle metal oxides signify a novel course of vital materials that are progressively being advanced for use in research and health-related applications. At the same time, we use Raman spectroscopy and fluorescence microscopic images for a better understanding of the effect of NPs on bacterial cells.

Keywords: Bacterial Assay; Pathogen *E-Coli*; SERS Raman; Fluorescence spectroscopy; Antibacterial study.
Received: 26 February 2022; Revised: 05 August 2022; Accepted: 29 August 2022.
Article type: Research article

1. Introduction

Metal oxides (MOs) nanoparticles (NPs), are rapidly being produced for use in research and health-related applications.[1-3] NPs are used as an alternative to antibiotics for attacking bacteria.[4,5] In general, metal NPs are unusual determinations in the fields of resolution[6] research[7] relative to mass materials[8] due to their high surface-to-volume ratio. In general, there were major biological activities and desirable structural properties of silver (Ag), gold (Au), and zinc (Zn) NPs.[9,10] Naturally, bacterial species are capable of developing resistance to antibiotics. Drug tolerance of bacteria causes pharmaceutical drugs to be unsuccessful in the treatment of many diseases.[11] Attention has been paid to antimicrobial metal NPs production.[12] Nowadays, with its ability to maintain antibacterial properties and durability during rugged and rough manufacturing while sustaining a healthy material for the human ecosystem, ZnO eco-friendly products are more focused on by researchers.[13,14] Owing to surface-bound water molecules, the aqueous nature of the suspensions of water and ZnO have mechanically improved ZnO's antimicrobial function, producing free radicals of oxygen and hydroxyl species accountable for exceptional stress from oxidation within handled bacterial cells. It is noted that ZnO-NPs serve as a possible antibacterial agent for the containment of *Escherichia coli* (*E. coli*). Other MOs such as Al_2O_3, SiO_2, and TiO_2 work very well against species of Subtilis and Pseudomonas.[15,16] Many Co (II) complexes and nanomaterials demonstrating antimicrobial activity have recently been synthesized.[17] However, reports show that

[1] *Central Research Laboratory, Dept. of Biotechnology, Sree Balaji Medical College & Hospital (SBMCH), Bharath Institute for Higher Education & Research (BIHER), Chennai-600073, Tamil Nadu, India.*

[2] *Laboratory of Integrative Multiscale Engineering Materials and Systems, Dept. of Aerospace Engineering, Indian Institute of Science, Bangalore-560012, India.*

[3] *Dept. of Physics, National Institute of Technology Calicut, Kozhikode-673601, Kerala, India.*

[4] *Dept. of Materials Science and Engineering, Advanced Materials Processing and Analysis Center, University of Central Florida, Orlando, FL, USA.*

[5] *Centre for Nanoscience & Technology, Pondicherry University, Puducherry, India.*

© Engineered Science Publisher LLC 2022

relative to the free ligand, the antibacterial properties of cobalt complexes are typically improved.[18] This appears to be the result of the metal's enhanced lipophilicity upon ligand coordination, which enables lipid bilayer permeability of the cell membrane, thus inhibiting metal binding sites on microorganism enzymes.[19] It is of considerable significance to synthesize compounds that inhibit bacterial growth and have low cytotoxicity, given the increase in bacterial diseases. The findings indicate that these nanomaterials, which can be conveniently and cost-effectively prepared, may be sufficient for the formulation of new forms of cobalt(III) complex bactericidal materials.[20,21] They contain the bidentate nitrogen ligand, bis[N-(2,6-di-isopropyl phenol)imino] acenaphthene (Pr-BIAN) which is known for its rigidity and strong antibacterial action. Another plasmon-induced effect is the plasmon-enhanced fluorescence (PEF) procedure, where the signal enhancement is attributed to two mechanisms: enhancement of excitation and enhancement of emissions.[22,23] A class of essential materials that are rapidly being produced for use in research and health-related activities are MOs and Au-NPs.[24] Au-NPs conjugates of antibiotics and antibodies were also used for the selective photothermal destruction of bacteria and protozoa.[25] Au-NPs affect antimicrobial activity, and further experiments are required to determine the exact mechanism involved in interactions with Au-NPs bacteria.[26] This experimental research aims to elucidate the antimicrobial action of the ZnO-NPs, Co-NPs, and Au-NPs against *E.coli* strain MTCC723. A fluorescence microscopic imaging study of *E. coli* MTCC 723 was investigated. Finally, surface-enhanced Raman spectroscopy (SERS) assessments were also conducted to grasp rapid, ultra-sensitive, and accurate quantitative detection of these pathogens.

2. Materials and approaches

2.1 Materials

Colonies were taken from MTCC with Fresh Pathogenic *E. coli* (National Centre for Cell Science). They are the pathogenic genetic stock, MTCC7233 (H-10407). For more analysis and sample preparation, *E. coli* was developed into a nutrient broth containing flasks already discussed in our previous article.[27] By dissolving the 28 gm of nutrient agar into 1000 mL of milli-Q-water. The above solution was autoclaved subsequently at 121 °C (15 lbs) for 30 min. The flask was then incubated in a shaking incubator at 37 °C at 110 g rpm for 24 h.

2.2 Chemicals and preparation of nanomaterials

Premium grade Au-NPs have been purchased from Reinste Nano Ventures Pvt. Ltd. Cobalt nanoparticles (99% pure) are purchased from Sigma Aldrich. The scale of the particles was about 50 nm. Co-NPs are suspended and mixed continuously in sterile regular saline until a uniform colloidal suspension is formed to reach a concentration of 500 mg·mL^{-1} powder. Sample of zinc oxide nanopowder (<100 nm) purchased from Sigma Aldrich were prepared as already discussed in our previous paper.[27] The scanning electron microscope has determined the surface morphology of ZnO nanopowder (SEM, FEI ESEM Quanta 200).

2.3 Inoculum test preparation and incubation

The single colony was taken with the aid of a circle from the stock bacterial population. Inoculation of this particular colony in a 100 mL flask containing 25 mL of clean nutrient broth. The flask was then incubated in a shaking incubator for 24 h at 37 °C and 115 rpm. After incubation, 0.4 mL of the overnight inoculum was transferred to a 100 mL flask containing 25 mL of nutrient broth and incubated at 37 °C and 100 rpm for 3-4 h in a shaking incubator. To achieve a mean target concentration of 1 × 10^5 colony-forming units·mL^{-1} to 1 × 10^5 colony-forming units·mL^{-1}, one mL was then diluted 3 times in nutrient broth serially (CFU·mL^{-1}). Sample processing has also been discussed in our earlier paper.[27] The number of bacteria in the 4 h culture was calculated by measuring the optical density of the culture at 660 nm.

2.4 Determination of the inhibition region

The agar well diffusion technique tested the antibacterial operations of the Co-NPs, Au-NPs, and ZnO-NPs. By autoclaving, Mueller Hinton agar medium was sterilized at 120 °C (15 lbs) and poured 30 mL per Petri dish. Sterilized cotton swab over solidified Mueller Hinton agar plates aseptically spread the 24 h broth culture. A separate concentration of ZnO-NPs (50, 75 and 100) (µg·mL^{-1}), Co-NPs (50, 75 and 100) (µg·mL^{-1}), and Au-NPs (50, 75 and 100) (µg·mL^{-1}) were applied to each Muller-Hinton agar medium for 20 µl of bacterial suspension and growth bacteria were tested on 37 °C culture media after 24 h of incubation (Fig. 2).

2.5 Imaging for bacterial culture and in-situ fluorescence:

2.5.1 Probe preparation

The staining probes SYTO 9 and Propidium Iodide (PI) were obtained from the company, Invitrogen. The 5 mg·mL^{-1} concentration was used for cell fluorescence imaging, and intensity and binding analysis using a plasmonic NP probe.

[6] *Integrated Composites Laboratory (ICL), Dept. of Chemical and Biomolecular Engineering, University of Tennessee, Knoxville, TN 37996, USA.*

[7] *Dept. of Inorganic and Physical Chemistry, Indian Institute of Science (IISc), Bangalore-560012, India.*

[8] *Indian Institute of Science Education and Research (IISER), Bhopal, MP, 462066, India.*

[9] *UNESCO-UNISA Africa Chair in Nanoscience/Nanotechnology, College of Graduate Studies, University of South Africa, Muckleneuk Ridge, P. O. Box 392, Pretoria, South Africa.*

[10] *Dept. of Physics, Government Arts & Science College, TUCAS Campus, Thennangur-604408, Thiruvalluvar University, Vellore, India.*

**Email:* zguo10@utk.edu (Z. Guo);
maniphysics@gmail.com (E . Manikandan)

© Engineered Science Publisher LLC 2022

The cultivated strains of *E. coli* MTCC723 were washed and suspended in phosphate buffer saline (PBS) with pH ~ 7.4 for experimental analysis. To capture the fluorescence images of each array, a fluorescence microscope (Carl Zeiss Axio Observer D1) equipped with a CCD camera (Axio Cam) with an excitation wavelength of 488 nm and an emission wavelength of 500-532 nm was used. The fluorescence intensity of each range of the recorded image is measured using the '*Image j* program' and the plasmonic effect is analyzed.

2.5.2 Sample preparation for Raman study

In vitro cells of the *E. coli* strain, MTCC 723 were allowed to expand until its Optical Density (OD) reaches 0.17. It joined the culture's lag phage, which for laboratory research is suitable for bacterial cells. Nanoparticles (ZnO-NPs, Au-NPs and Co-NPs) with the concentration of 10 $m.mol^{-1}$ were added in to the cells. The cells were centrifuged at 12000 rpm for 30 min. As a comparative study, Raman spectroscopic characterization with controlled concentration was conducted. After vertexing, an aliquot containing 2 µL of the mixture was lowered onto a Raman-compliant magnesium fluoride (MgF_2) slide and air-dried under atmospheric conditions for further Raman spectroscopic tests.

2.5.3 Raman instrumentation

To perform the Raman measurements a Renishaw inVia Raman microscope equipped with 1200 lines/mm grating was used. The Raman spectrum was recorded using an excitation wavelength of 633 nm from the He-Ne laser. The Raman spectra of samples were collected using a ×100 objective (0.8 NA) and the same was used for the collection of the backscattered light from the sample. The spectrometer was calibrated before collecting the Raman spectra using a silicon 520.5 cm^{-1} line. The scattered signals were detected using a Peltier-cooled CCD camera. All the Raman spectra were obtained at normal room temperature (RT) using 60 s of acquisition time and at each position, two spectra were collected and co-added.

3. Outcome and discussion

3.1 Characterization of ZnO-NPs, Co-NPs, and Au-NPs

The SEM study showed the structural morphology of ZnO-NPs, Au-NPs, and Co-NPs. The nanoparticles distribution is shown in Figs. 2(a-c). As seen in (Fig. 2(a)), ZnO-NPs have been defined by SEM. The scale of the ZnO-NPs is approximately 250-300 nm and the particles have either a rod-like or spherical shape. The Au-NPs size is in the range of 250-300 nm (Fig. 2(b)) and shows a circular and hexagonal configuration in terms of shape. The Co-NPs are connected with uneven pore dimensions and shapes (Fig. 2(c)) and the scale of the Co-NPs is approximately 50 nm. Fig. 1 illustrates the interaction between NPs and *E. coli* cells.

3.2 Antibacterial study

Less than 0-20 percent drop imply no bactericidal impact, according to the bacterial reduction efficiency study; 20-50 percent decrease indicate an ineffective bactericide; 50-70 percent decreases indicate an articulate bactericide; more than 70 percent decrease show a strong bactericidal effect.[28,29] Under these criteria (Fig. 3(a) & Table 1), 50 $\mu g \cdot mL^{-1}$ concentration of ZnO displays no bactericidal effect. However, plates with a concentration of 75 $\mu g \cdot mL^{-1}$ displays articulate bactericidal effect (50% drop) and plates with 100 $\mu g \cdot mL^{-1}$ concentration has a powerful bactericidal expressive effect. Based on these findings, ZnO-NPs demonstrated an inhibition zone (mm) of approximately 16 nm, 20 nm, and 22 mm in diameter for concentrations of 50 $\mu g \cdot mL^{-1}$, 75 $\mu g \cdot mL^{-1}$, and 100 $\mu g \cdot mL^{-1}$, respectively. For the gram-negative strains of *E. coli*, ZnO nanoparticles have an articulate antibacterial effect. *E. coli* was used to determine the antibacterial effect of the synthesized ZnO nanoparticles at various concentrations. The *E. coli* isolates (Table 1) show how various concentrations of ZnO nanoparticles display the inhibition zone. The *E. coli* ZnO cells exhibit less absorption than a single bacterial cell. The binding mechanism between ZnO-NPs and bacterial cells is not yet clear. The plausible mechanisms are (i) the release of Zn^{2+} in the broth added substantially to the overall antibacterial impact of nanoparticles of zinc oxide[29] and (ii) the close interaction of ZnO with bacterial cell walls.[30] The tuned nanoparticles cause the degradation to the integrity of bacterial cells[31] and the creation of reactive oxygen species (ROS).[32] In the case of Au-NPs (Fig. 3(b) & Table 1), with a rise in nanoparticle concentration of 100 $\mu g.mL^{-1}$, Au-NPs

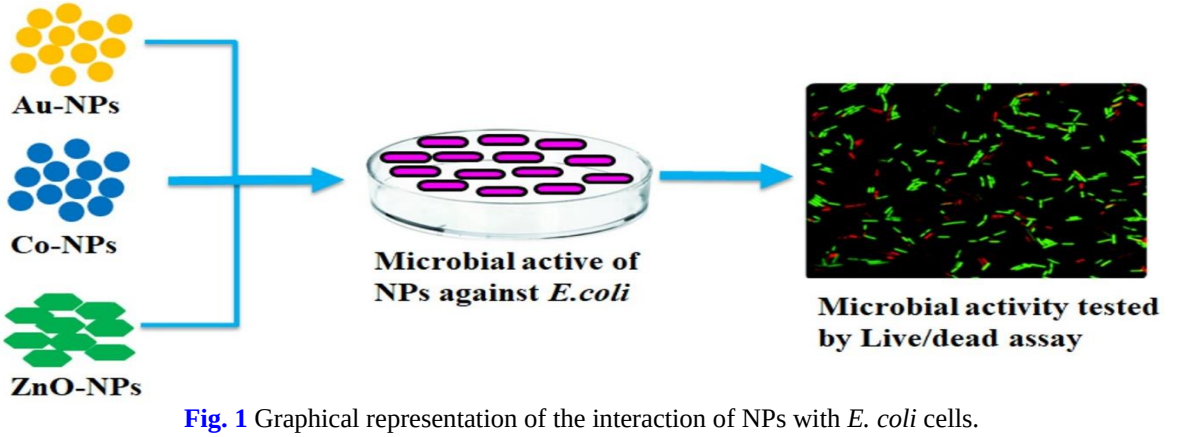

Fig. 1 Graphical representation of the interaction of NPs with *E. coli* cells.

© Engineered Science Publisher LLC 2022

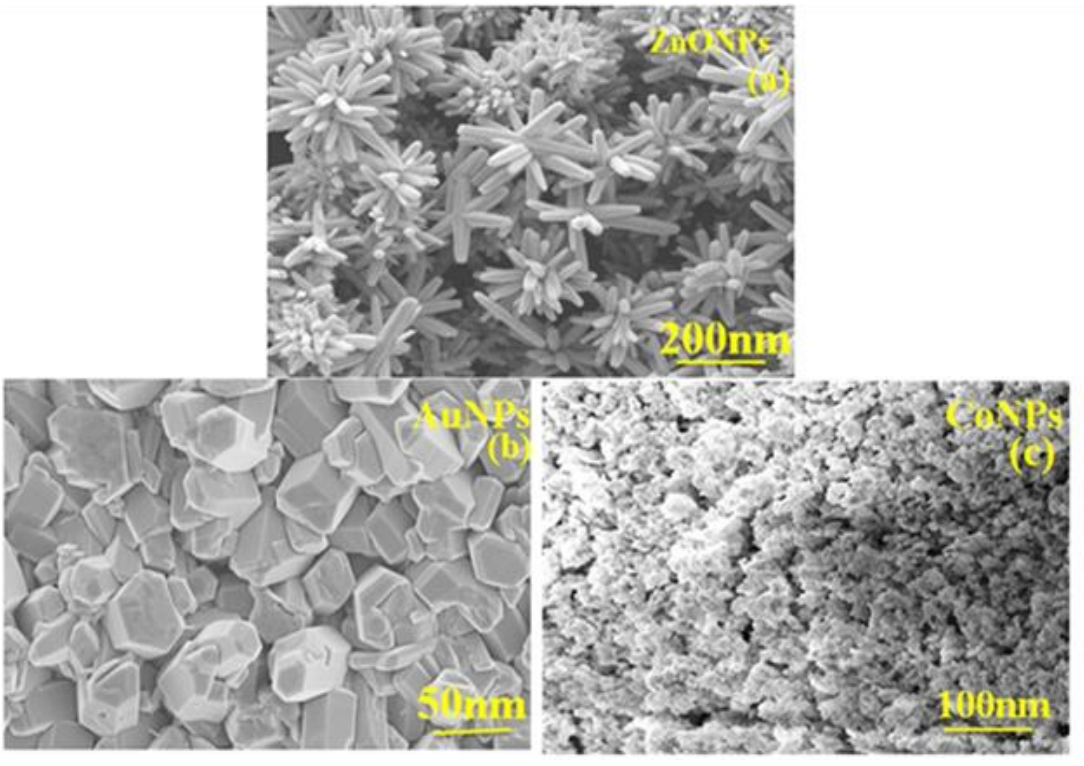

Fig. 2 (a-c) FE-SEM images of (a) ZnO-NPs; (b) Au-NPs; and (c) Co-NPs.

have more bactericidal activity and display articulate bactericidal effect in plates. Based on these findings, the articulate antibacterial activity of gram-negative *E. coli* cell s is expressed by Au-NP nanoparticles. Strains of *E. coli* were studied for the antibacterial effect of the prepared Au-NPs nanoparticles at various concentrations. Isolates of *E. coli* are shown in Fig. 3(b). Various amounts of metal nanoparticles were seen in the inhibition region. Results revealed that Au-NPs had an inhibition zone (mm) of approximately 18 nm, 21 nm, and 24 mm in diameter at the concentration of 50, 75 and 100 $\mu g \cdot mL^{-1}$, respectively. Some processes may be responsible for the bactericidal activity of Au-NPs; the optical properties of conductive NPs, such as those made of gold, have been correlated with surface plasmon resonance (SPR). (1) In the broth, the release of Au-NPs significantly contributed to the overall antibacterial effect,[33] and (2) the strong association between Au-NPs and bacterial cell walls. The tuned nanoparticles cause the degradation of the bacterial cell integrity[34] and the development of ROS,[35] a photothermal effect resulting from the special property of a nanoscaled gold colloidal solution with a heavily enhanced absorption optical band at 530 nm corresponding to the oscillations of Au-NPs' surface plasmon resonance (SPR). In contrast to plates containing 50 $\mu g \cdot mL^{-1}$ concentration, (Fig. 3(c) & Table 1) 100 $\mu g \cdot mL^{-1}$ Co-NPs had more bactericidal effects than plates containing 50 $\mu g \cdot mL^{-1}$ concentration, however the 75 $\mu g \cdot mL^{-1}$ reveals 30 percent and 50 percent of antibacterial effect signifies articulate bactericidal effects. From these findings, it can be processed that cobalt nanoparticles feature a Gram-negative sensitive antiseptic effect. The antibacterial activity of the cobalt nanoparticle on *E. coli* cells has been studied at various concentrations. Isolates of *E. coli* in Fig. 3(c) demonstrated the different concentrations of metal nanoparticles in the inhibition region.

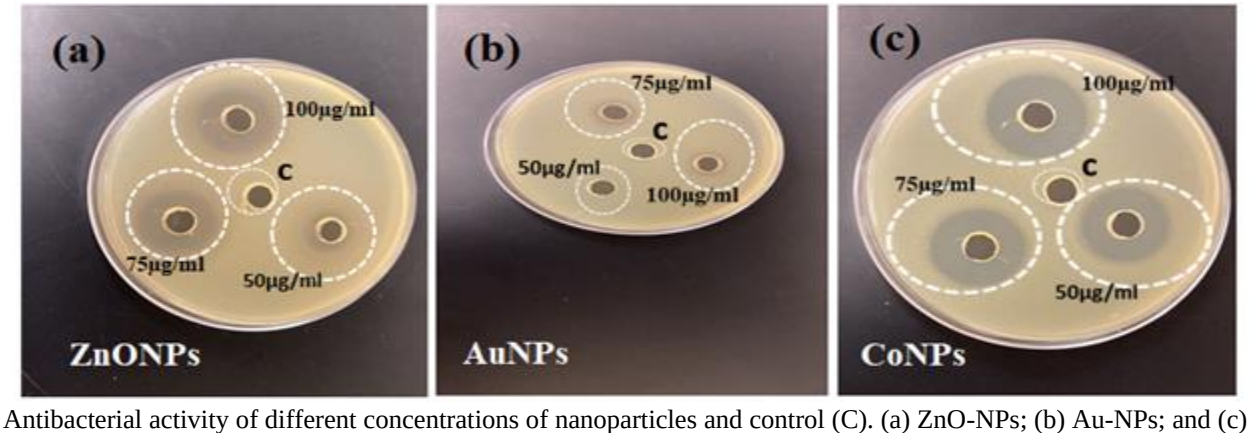

Fig. 3 Antibacterial activity of different concentrations of nanoparticles and control (C). (a) ZnO-NPs; (b) Au-NPs; and (c) Co-NPs against *E. coli* cells.

 © Engineered Science Publisher LLC 2022

Results revealed that cobalt had an inhibition zone (mm) of approximately 22, 26, and 32 mm in diameter for 50 $\mu g \cdot mL^{-1}$, 75 $\mu g \cdot mL^{-1}$, and 100 $\mu g \cdot mL^{-1}$, respectively. The toxic effect of the cobalt nanoparticle in the absorbance sample was well known. The *E. coli* with Co-NPs exhibits less absorption than that of the only bacterial cell, *E. coli* cell. From the optimizing of Co-NPs with the bacterial cells, the binding properties of Co-NPs with bacterial cells are still not evident, but the key reason is associated with the behavior in (1) the chelated complex in which the lipophilic application of the metal is increased and its infusion is ordered above the lipid layers of the bacterial membranes;[36] (2) the positive charge of the interaction of the metal dipole-dipole is partially conjugated with the supporter atoms existing within the ligands while the delocalization of the π-electron occurs; and (3) other factors such as dipole moment, conductivity and solubility, which are predisposed to the latency of the metal ions, are also possible to display the inhibitory activity of Co-NPs to develop.

Table 1. Zone of inhibition of *E. coli* cells with different nanomaterial.

ZnO Nanoparticle (µg/mL)	Zone of Inhibition (mm)
50	16
75	20
100	22
Cobalt Nanoparticles (µg/mL)	**Zone of Inhibition (mm)**
50	22
75	26
100	32
Gold Nanoparticles (µg/mL)	**Zone of Inhibition (mm)**
50	18
75	21
100	24

3.3 Microscopic examination of fluorescence

The goal of this research is to investigate the effect of contagious *E. coli* cells with ZnO-NPs, Co-NPs and Au-NPs. As seen in Fig. 2(a), ZnO-NPs are distinguished from FE-SEM imaging. Au-NPs are procured from Reinste nano Projects Pvt. Ltd. The structure and dimensions were characterized through FE-SEM imaging with a spherical shape of some 50 nm (Fig. 2(b)). Co-NPs were also procured from Reinste nano Ventures Pvt Ltd. FE-SEM image depicted that Co-NPs are spherical with the diameter of ~100 nm. For the procedure, cells were suspended in a phosphate buffer (pH ~ 7.4). Double dyes, propidium halide, and SYTO nine (LIVE/DEAD Backlight microorganism Viability package, Invitrogen) stained the cells. Due to the effect of area field enhancement and the increased emission rate by surface plasmon coupled emission, the process of plasmon improvement exhibits increased excitation rate, which could boost the light intensity and quantum yield.

To determine the effect of ZnO-NPs, Co-NPs and Au-NPs on *E. coli* cells, both nutrient media cultures were inoculated with cells MTCC 723, each containing the 10 $m \cdot mol^{-1}$ ZnO-NPs, 10 $m \cdot mol^{-1}$ AuNPs, and 10 $m \cdot mol^{-1}$ Co-NPs. These sets were incubated at 37 °C for a long time inside the apparatus. From the light micrographs, improvements were confirmed within the integrity and viability assay of the cellular membrane. The cytomembrane transfuses the binding of nucleic acid to the fluorescent probe until the microorganism cell region unit is exposed to the light probe. Compared to nanoparticles (ZnO-NPs, Au-NPs, and Co-NPs), the light strength of 2 cell area units is shown in Figs. 4(a-d). Analysis of the images was done by the Zeiss image processing software framework, "Image j software" exploitation. In the presence of SYTO nine and Propidium iodide probe stain, the effect of Au-NPs, ZnO-NPs, and Co-NPs on the viability of the MTCC723 strains was analyzed by microscopy. Fig. 4 displays the light images of (a) MTCC723, (b) MTCC723 in the presence of Au-NPs (10 $m.mol^{-1}$), (c) MTCC 723 in the presence of ZnO-NPs (10 $m.mol^{-1}$) and (d) MTCC 723 in the presence of Co-NPs (10 $m.mol^{-1}$). SYTO nine probe stains living cells that present as a novice in color and PI stains dead cells that appear red are observed in Fig. 4. Staining reports recommend that in the presence of Au-NPs (10 $m.mol^{-1}$), MTCC723 greatly shows the improvement of *E. coli* cells (Fig. 4(b)). The following (1) Au-NPs polarize with opposite charges within the center and even the surface that causes a dipole oscillation between several different modes of Plasmon resonances at different wavelengths and (2) excitation of Au-NPs at explicit wavelengths ends up in the fluorophore (FL) surface charge exchange.[37,38] The expansion of MTCC723 (Fig. 4(c)) would be considerably hindered by ZnO-NPs of 10 $m.mol^{-1}$. In two pathways, ZnO affects the microorganism cells by binding to membranes, interfering with their ability and integrity, and inducing ROS production.[39,40] ROS causes damage to any or more of the macromolecules in the cells by extreme aerophilic tension, resulting in supermolecule peroxidation, protein modification, enzyme inhibition, and RNA and mutations.[41] As a result of the increasing Zn^{2+} ions inside the bacteria and the hook-up of ZnO-NPs there is harm to the microorganism cytomembrane.[42] The detrimental consequence of the resulting nano-bacterial surface potential on microorganism survivability was confirmed by colony-forming unit and potential neutralization tests. The positive surface potential of ZnO-NPs improves the assembly of the reactive element species and imposes mechanical membrane stress while communicating with the negative surface potential of the microorganism membrane, contributing to membrane depolarization.[42] Co-NPs nanoparticles, on the other hand, also illustrate the restrictive effect of micro-organism cells (Fig. 4(d)). The poorer viability of the cell is attributed to the modified cytomembrane permeability and metabolic mechanism of living things inside the cell of the microorganism induced by Co-NPs. NPs' therapeutic drug activity coincides with their dosage and size.[43] The

© Engineered Science Publisher LLC 2022

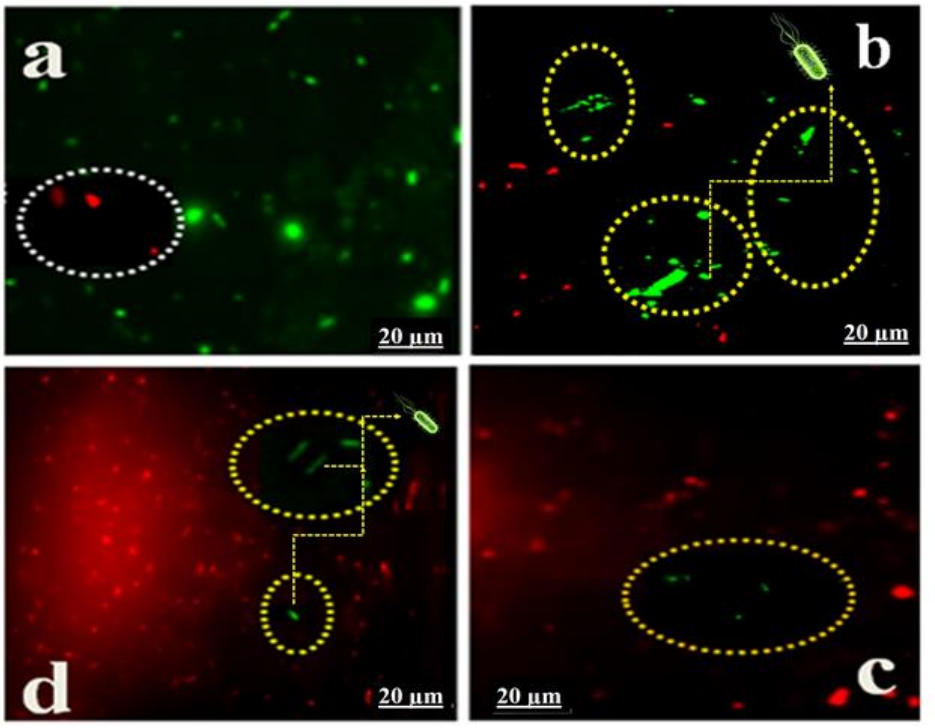

Fig. 4 Fluorescence images of *E.coli* bacteria strains, (a) MTCC723; (b) MTCC723 in presence of Au-NPs (10 m.mol^{-1}); (c) MTCC723 in presence of ZnO-NPs (10 m.mol^{-1}); (d) MTCC 723 in presence of Co-NPs (10 m.mol^{-1}).

antimicrobial propensity of nanoparticles of metal compounds mostly depends on the surface potential, the potential arising from the contact of the surface of the nanoparticle with the membrane of the microorganism.[44,45] One of the major reasons for NPs, aside from the SPR below incident lightweight, is that the molecular charge and particles within the NP-cell suspension will produce entirely different force fields and alter the transport properties of ion channel particles within the cell walls.[46] Co-NPs, depending on the measurements and also the exact distance between the dye and Co-NPs[47] may boost or quench the dye light. Measured intensities suggest that the fluorescent strength of the microorganism cells improved for clamped Co-NPs with a median diameter of 20 nm. This is also attributed to the gift of the Co-NPs inside the cell suspension's surface plasmon effect.[48,49] Any studies indicate the factors behind the enhancement of the subsequent *E.coli* fluorescent intensity region unit. (1) *E. coli* contains a semi-permeable membrane composed of supermolecules, lipopolysaccharide, and peptidoglycan, active oxides formed by a primary solid solution. Nanopowders have an additional potential to infiltrate the semi-permeable membrane and decrease the biological process of From *E. coli*. In addition, the Co-NPs polarize with opposite charges from the center and even the surface that produces a dipole oscillation at various wavelengths and wavelengths between several different types of plasmon resonances. (2) The real fact is that the operation progressed within the chemical action, the charge of the metal is partially exchanged with the gift of the donor atoms within the ligands. Another possibility would be the full chelate ring. These circumstances would successively raise the lyophilic character of the metal chelate and facilitate its permeation across the membranes of the microorganism's macromolecule layers. It is often believed that Co-NPs show strong reaction potential within the medium of living things due to the association of Co-NPs with amino acids.[50,51] The Co^{2+} induced toxicity in *E. coli* by enhancing aerophilic stress, inhibiting enzyme activity, decreasing cytosolic iron content, decreasing total PL content, increasing supermolecule peroxidation, and increasing CL content.

3.4 Raman microscopic study

Being a molecular fingerprint tool, micro-Raman spectroscopy (µ-RS) provides valuable molecular information about the morphology and biochemical constituents of the bacterial cell. To get more details about the interaction between bacterial cells (MTCC723) and NPs (ZnO, Au, Co), we have carried out the Raman measurements on the control and NP-treated bacterial cell samples. The average and normalized Raman spectra in the range of 500 – 1710 cm^{-1} for the control and NP treated bacterial cells along with their Raman difference spectra for MTCC723 cells are shown in Fig. 5. Very accurate assignments of the Raman peaks of a bacterial cell are not easy because of the significant overlapping of various peaks due to its complex cellular components. Since, proteins, lipids, nucleic acids and carbohydrates are the main cellular components; the peaks that appear in the Raman spectrum can be attributed to these constituents.[52] A tentative assignment of the peaks is tabulated in Table 2. We have characterized the interaction between NPs and bacterial cells based on variation in the intensity of the peaks because the analysis based on peak position is insignificant due to

 © Engineered Science Publisher LLC 2022

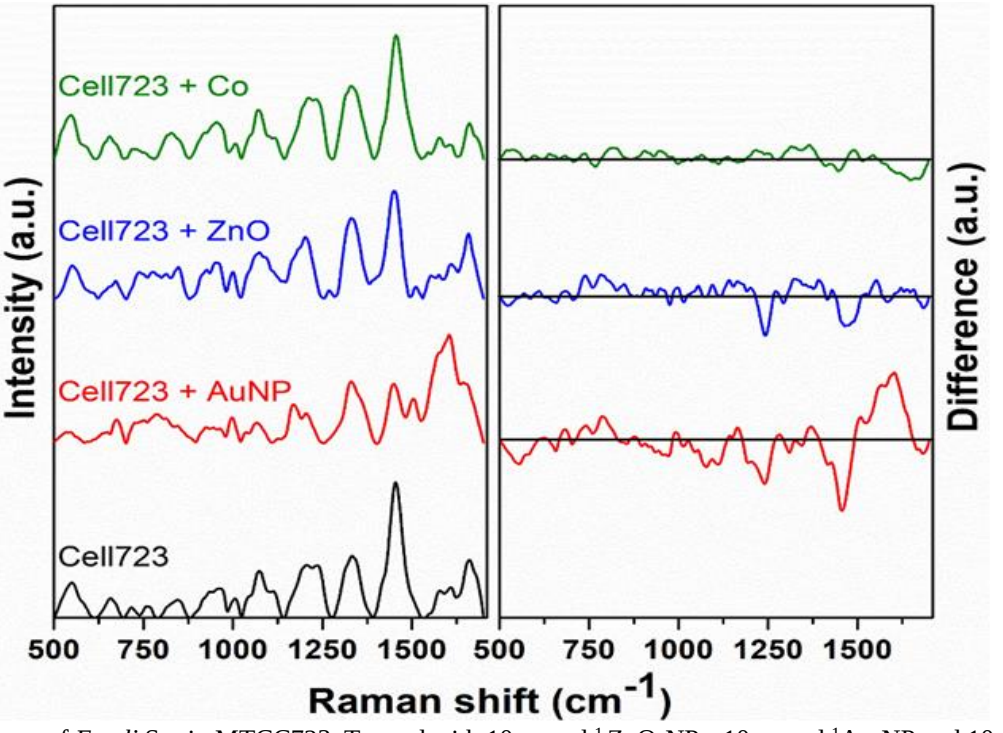

Fig. 5 Raman spectra of *E.coli* Strain MTCC723. Treated with 10 m.mol^{-1} ZnO-NPs, 10 m.mol^{-1}Au-NP and 10 m.mol^{-1} Co-NPs.

Table 2. A tentative assignment of Raman modes for *E. coli*, taken from Fig. 5.

Raman modes (in cm^{-1})	Assigned Biomolecules
540 (s)	Protein (S-S stretching)
655 (m)	DNA/RNA
717 (w)	DNA/RNA
772 (w)	DNA/RNA
845 (m)	Proteins
915 (sh)	(C-O-C) skeletal mode
971 (w)	Proteins/Lipids
1007 (w)	Proteins
1041 (sh)	Proteins/Polysaccharides
1075 (m)	DNA/RNA
1121 (w)	Proteins/Carbohydrates/Lipids
1220 (s)	DNA/RNA/ Proteins
1329 (s)	Proteins/DNA/RNA
1453 (vs)	Lipids
1580 (sh)	DNA/RNA
1611 (s)	Proteins
1659 (s)	Proteins

vs: very strong, s: strong, m: medium, w: weak, sh: shoulder

extensive overlapping of the bands. Also, for similar kinds of species, the biochemical constituents are almost the same and the only difference is their concentrations, which varies the intensity of the peaks and not the position.

Figure 5 shows the Raman spectra of the control samples. It is very clear that except a few minor changes due to their concentrations in the biochemical constituents both the control samples possess similar Raman features. Although the control samples show similar spectral characteristics after the NP treatment the bacterial cells display several noticeable differences as depicted in Fig. 5. The presence of different cellular components in the cells and the distinct mechanism involved in the interaction with Au, ZnO and Co NPs could be the plausible cause of this spectral variability. A detailed analysis of the spectral features corresponding to different functional groups can be utilized to extract several biochemical information about the cell from the Raman spectrum, particularly the aspects of the cellular membrane.

The interaction between these *E. coli* strains and two NPs (Au and ZnO) has already been discussed thoroughly in our previous paper.[52,53] Several changes were observed in the Raman spectral profiles of biochemical components of both bacterial strains. Major changes were observed in the protein and lipid bands as compared to the band assigned to nucleic acids (DNA/RNA). However, Au-NPs showed enhanced changes as compared with ZnO-NPs for both the bacterial cells which were evident from the Raman spectra and Raman difference spectra as well. These enhanced changes were attributed to the SPR of Au-NPs which is absent in ZnO-NPs. From a detailed Raman spectral analysis, the NP-induced conformational changes of lipids, proteins and nucleic acids were observed and indicated the possible cell death.

In this current study, we have aimed to give a comparative study on the antibacterial properties of Au-NPs, Co-NPs and ZnO-NPs. Since each type of NP has its interaction mechanism with the bacterial cells, the Raman spectra depict changes in peak profiles (intensity, position and line width) for various spectral features in a different manner that are visible (as shown in Fig. 5). While we did not characterize the specific chemical changes because of each NP treatment, we focused on differences in signature to distinguish their interaction a

© Engineered Science Publisher LLC 2022

Table 3. A change in magnitude of the intensity of three marker bands.

Raman modes (cm^{-1})		Magnitude of variation in intensity		
Biochemicals Signatures	Peak Position	Au-NPs MTCC723	ZnO-NPs MTCC723	Co-NPs MTCC723
Proteins	1659	↓	↓	↓
Lipids	1453	↓	↓	↓
DNA/RNA	1220	↓	↓	↑

Up Arrow: Increment; Down Arrow: Decrement

mechanisms. Several marker bands assigned to different biochemical constituents such as proteins vibrational modes (1659, 1611, 1329 and 540 cm^{-1}), DNA/RNA (1220 cm^{-1}) and lipids (1453 cm^{-1}) show a drastic change in spectral profiles of treated *E. Coli* strain with NPs as compared to their control samples, which are evident from the Raman spectra (Fig. 5). However, we have selected only three marker bands, 1659,1453 and 1220 cm^{-1} correspond to proteins, lipids and DNA/RNA, respectively in our further analysis to study the interactions. The magnitude of the change in intensity of these three marker bands is tabulated in Table 3. Almost similar kind of changes are observed in the Raman spectral features of these three marker bands for both *E. coli* strains when treated with ZnO-NPs and Au-NPs as we have already seen in our previous study,[38,53,54] which confirm the same interaction mechanism of these two NPs with these two bacterial cells. After the Co-NPs treatment, the two bacterial strains show almost similar spectral changes (i.e., decrease in intensity) for both the protein and lipid marker bands. But a substantial intensity increase at 1220 cm^{-1} (DNA/RNA marker band) is observed as compared to the cells treated with ZnO-NPs and Au-NPs. The enhanced chelating activity of the Co-NPs could be the plausible reason which favors its penetration through the cell walls and inturn, induces cytotoxicity by preferably interacting with the nucleus and altering its structural form.[55] To get more insight and details about the interactions, a difference is obtained by subtracting the average Raman spectra of controlled bacterial samples from the NP-treated bacterial samples. Fig. 5 depicts the difference spectra for both bacterial strains. As evident from Fig. 5, there are remarkable differences (deviation from the black solid control line shown in Fig. 5) observed between these NP-treated samples. Several prominent positive and negative structures indicate the change in intensity of the Raman features corresponding to different cellular components which imply the extent of changes in a bacterial cell due to the NP treatments. Among the three NPs, the most changes occur in the protein and lipid compositions for Au-NPs treated cells in comparison to both the control samples. On the other hand, ZnO-NPs treated cells show moderate changes in protein and lipid compositions. The DNA/RNA composition-related changes are very less as compared to the other two compositional changes in these two ZnO-NPs and Au-NPs treated samples. But, substantial DNA/RNA compositional changes appear in the Co-NPs treated cells as compared to the same when treated with ZnO-NPs and Au-NPs. This is possibly the result of cell-specific interaction mechanisms which vary from NP to NP as already well-established in the literature.

The changes are observed in the spectral profiles of the Raman marker bands of protein, lipid and DNA/RNA of *E. coli* strain MTCC723, but their magnitude varies with NPs as seen clearly from the Raman and Raman difference spectra, respectively. However, protein and lipid changes are more dominant than the changes observed for DNA/RNA in the case of Au-NPs and ZnO-NPs treated samples. The detailed interaction mechanism of Au-NPs and ZnO-NPs with bacterial cells is already discussed in our previous paper. Interestingly, Co-NPs treated samples show much pronounced DNA/RNA changes which are comparable with that of protein and lipid in magnitude. Germane to this study, the bacterial cells treated with Co-NPs show major DNA/RNA changes as compared to the other two NPs. Already, the experimental results show a high antibacterial activity of Co-NPs against *E. coli* cells due to its enhanced chelation property which is very much effective to inhibit the growth of bacteria.[56,57] The higher chelating activity of the Co-NPs favors its penetration through the lipid membrane of the cell walls. Our observations suggest the prominent Co-NPs induced changes in the DNA/RNA which alter its structural form by mutilating their helical structure and leading to possible cell death.

4. Conclusion

Our approach can realize ultra-sensitive rapid detection of *E. coli* whole cell on facets of in vitro study quantitation and qualitative detection method. Results indicated the high efficiency of nanoparticles to inhibit the growth of such

 © Engineered Science Publisher LLC 2022

pathogenic microorganisms. Nanoparticle metal oxides signified a novel course of vital materials that are progressively being advanced for use in research and health-related applications. At the same time, we used Raman spectroscopic and Fluorescence imaging studies for the sensitive detection of pathogenic *E. coli* cells. We used ZnO-NPs, Au-NPs, and Co-NPs for *E. coli* cell detection. Co-NPs provided an owing antibacterial effect with low concentration against Gram-negative *E. coli* cells. Thus, Co-NPs could be used as an encouraging antibacterial agent in biomedical applications.

Acknowledgments

The author Gargibala would like to thank the research program generously supported by Central Research Laboratory, Sri Balaji Medical College & Hospital, BIHER, Respected Chairman Thiru. S. Jagathrakshakan, *M.P. Ex.Central Minister*, Er. N. Elamaran, Managing Director, Dr J. Sri Nisha continuous encouragement and, scientific-technical aid from the UNESCO-UNISA Africa Chair in Nanosciences and Nanotechnologies (U2ACN2), the National Research Foundation of South Africa (NRF), the University of South Africa, iTemba LABS-NRF, the National Laser Centre of South Africa (NLC) via the Nanosciences Africa Network (NANO-AFNET) as well as the African Laser Centre (ALC) to whom we are grateful. GS and DRM thankfully acknowledge financial support through IDC-Water project under the 2+2 program of Indo-German Science and Technology Centre (IGSTC). Dr. E. Manikandan, thanks to UNESO-UNISA Nanosciences/Nanotechnology and TNSCST, STPC (2020-2021) Scheme Project Related Grant scheme on Fingerprint Raman Spectroscopic Techniques for Pandemic Samples Analysis and Thereof.

Conflict of interest

The authors declare no conflict of interest.

Supporting information

Not Applicable.

References

[1] S. Cheeseman, A. J. Christofferson, R. Kariuki, D. Cozzolino, T. Daeneke, R. J. Crawford, V. K. Truong, J. Chapman, A. Elbourne, Antimicrobial metal nanomaterials: from passive to stimuli-activated applications, *Advanced Science*, 2020, **7**, 1902913, doi: 10.1002/advs.201902913.

[2] D. Krewski, R. A. Yokel, E. Nieboer, D. Borchelt, J. Cohen, J. Harry, S. Kacew, J. Lindsay, A. M. Mahfouz, V. Rondeau, Human health risk assessment for aluminium, aluminium oxide, and aluminium hydroxide, *Journal of Toxicology and Environmental Health, Part B*, 2007, **10**, 1-269, doi: 10.1080/10937400701597766.

[3] E. Sánchez-López, D. Gomes, G. Esteruelas, L. Bonilla, A. L. Lopez-Machado, R. Galindo, A. Cano, M. Espina, M. Ettcheto, A. Camins, A. M. Silva, A. Durazzo, A. Santini, M. L. Garcia, E. B. Souto, Metal-based nanoparticles as antimicrobial agents: an overview, *Nanomaterials*, 2020, **10**, 292, doi: 10.3390/nano10020292.

[4] H. A. Hemeg, Nanomaterials for alternative antibacterial therapy, *International Journal of Nanomedicine*, 2017, **12**, 8211-8225, doi: 10.2147/IJN.S132163.

[5] Y. Wang, Q. Yuan, W. Feng, W. Pu, J. Ding, H. Zhang, X. Li, B. Yang, Q. Dai, L. Cheng, J. Wang, F. Sun, D. Zhang, Targeted delivery of antibiotics to the infected pulmonary tissues using ROS-responsive nanoparticles, *Journal of Nanobiotechnology*, 2019, **17**, 1-16, doi: 10.1186/s12951-019-0537-4.

[6] V. Schroeder, S. Savagatrup, M. He, S. Lin, T. M. Swager, Carbon nanotube chemical sensors, *Chemical Reviews*, 2019, **119**, 599-663, doi: 10.1021/acs.chemrev.8b00340.

[7] K. Yang, Q. Han, B. Chen, Y. Zheng, K. Zhang, Q. Li, J. Wang, Antimicrobial hydrogels: promising materials for medical application, *International Journal of Nanomedicine*, 2018, **13**, 2217-2263, doi: 10.2147/IJN.S154748.

[8] J. Xue, T. Wu, Y. Dai, Y. Xia, Electrospinning and electrospun nanofibers: methods, materials, and applications, *Chemical Reviews*, 2019, **119**, 5298-5415, doi: 10.1021/acs.chemrev.8b00593.

[9] A. Gentile, F. Ruffino, M. G. Grimaldi, Complex-morphology metal-based nanostructures: fabrication, characterization, and applications, *Nanomaterials*, 2016, **6**, 110, doi: 10.3390/nano6060110.

[10] Y. Xia, Y. Xiong, B. Lim, S. E. Skrabalak, Shape-controlled synthesis of metal nanocrystals: simple chemistry meets complex physics, *Angewandte Chemie International Edition*, 2009, **48**, 60-103, doi: 10.1002/anie.200802248.

[11] N. Narayan, A. Meiyazhagan, R. Vajtai, Metal nanoparticles as green catalysts, *Materials*, 2019, **12**, 3602, doi: 10.3390/ma12213602.

[12] K. S. Siddiqi, A. Husen, R. A. K. Rao, A review on biosynthesis of silver nanoparticles and their biocidal properties, *Journal of Nanobiotechnology*, 2018, **16**, 14, doi: 10.1186/s12951-018-0334-5.

[13] P. Singh, S. Pandit, J. Garnæs, S. Tunjic, V. R. Mokkapati, A. Sultan, A. Thygesen, A. Mackevica, R. V. Mateiu, A. E. Daugaard, A. Baun, I. Mijakovic, Green synthesis of gold and silver nanoparticles from Cannabis sativa (industrial hemp) and their capacity for biofilm inhibition, *International Journal of Nanomedicine*, 2018, **13**, 3571-3591, doi: 10.2147/IJN.S157958.

[14] W. Liu, P. Su, A. Gonzales, N. Wang, Z. Zhang, H. Li, T. J. Webster, J. Wang, S. Chen, Optimizing stem cell functions and antibacterial properties of TiO2 nanotubes incorporated with ZnO nanoparticles: experiments and modeling, *International Journal of Nanomedicine*, 2022, **17**, 463-464, doi: 10.2147/IJN.S359722.

[15] M. J. Nasiri, M. Haeili, M. Ghazi, H. Goudarzi, A. Pormohammad, A. A. Imani Fooladi, M. M. Feizabadi, New insights in to the intrinsic and acquired drug resistance mechanisms in mycobacteria, *Frontiers in Microbiology*, 2017, **8**, 681, doi: 10.3389/fmicb.2017.00681.

[16] M. Álvarez-Paino, A. Muñoz-Bonilla, M. Fernández-García, Antimicrobial polymers in the nano-world, *Nanomaterials*, 2017,

© Engineered Science Publisher LLC 2022

7, 48, doi: 10.3390/nano7020048.
[17] E. Pahon, D. C. Ilie, S. Shova, C. Oprean, V. Păunescu, O. T. Olaru, F. Rădulescu, A. Gulea, T. Ro, D. Drăgănescu, Synthesis, characterization, antimicrobial and antiproliferative activity evaluation of Cu(II), Co(II), Zn(II), Ni(II) and Pt(II) complexes with isoniazid-derived compound, *Molecules*, 2017, **22**, 650, doi: 10.3390/molecules22040650.
[18] Y. Yan, J. Zhang, L. Ren, C. Tang, Metal-containing and related polymers for biomedical applications, *Chemical Society Reviews*, 2016, **45**, 5232-5263, doi: 10.1039/c6cs00026f.
[19] E. L. Chang, C. Simmers, D. A. Knight, Cobalt complexes as antiviral and antibacterial agents, *Pharmaceuticals*, 2010, **3**, 1711-1728, doi: 10.3390/ph3061711.
[20] E. Bossi, D. Zanella, R. Gornati, G. Bernardini, Cobalt oxide nanoparticles can enter inside the cells by crossing plasma membranes, *Scientific Reports*, 2016, **6**, 22254, doi: 10.1038/srep22254.
[21] H. Nikaido, Molecular basis of bacterial outer membrane permeability revisited, *Microbiology and Molecular Biology Reviews*, 2003, **67**, 593-656, doi: 10.1128/MMBR.67.4.593-656.2003.
[22] S. S. Fuglerud, K. Milenko, A. Aksnes, D. R. Hjelme, Surface-enhanced absorption spectroscopy for optical fiber sensing, *Materials*, 2019, **13**, 34, doi: 10.3390/ma13010034.
[23] D. S. Ahmed, M. K. A. Mohammed, Studying the bactericidal ability and biocompatibility of gold and gold oxide nanoparticles decorating on multi-wall carbon nanotubes, *Chemical Papers*, 2020, **74**, 4033-4046, doi: 10.1007/s11696-020-01223-0.
[24] J. H. Lee, H. Y. Cho, H. K. Choi, J. Y. Lee, J. W. Choi, Application of gold nanoparticle to plasmonic biosensors, *International Journal of Molecular Sciences*, 2018, **19**, 2021, doi: 10.3390/ijms19072021.
[25] Y. Zhou, Y. Kong, S. Kundu, J. D. Cirillo, H. Liang, Antibacterial activities of gold and silver nanoparticles against Escherichia coli and bacillus Calmette-Guérin, *Journal of Nanobiotechnology*, 2012, **10**, 19, doi: 10.1186/1477-3155-10-19.
[26] A. Elbehiry, M. Al-Dubaib, E. Marzouk, I. Moussa, Antibacterial effects and resistance induction of silver and gold nanoparticles against Staphylococcus aureus-induced mastitis and the potential toxicity in rats, *MicrobiologyOpen*, 2019, **8**, e00698, doi: 10.1002/mbo3.698.
[27] G. Satpathy, G. K. Chandra, E. Manikandan, D. R. Mahapatra, S. Umapathy, Pathogenic Escherichia coli (E. coli) detection through tuned nanoparticles enhancement study, *Biotechnology Letters*, 2020, **42**, 853-863, doi: 10.1007/s10529-020-02835-y.
[28] B. Ahmed, F. Ameen, A. Rizvi, K. Ali, H. Sonbol, A. Zaidi, M. S. Khan, J. Musarrat, Destruction of cell topography, morphology, membrane, inhibition of respiration, biofilm formation, and bioactive molecule production by nanoparticles of Ag, ZnO, CuO, TiO_2, and Al_2O_3 toward beneficial soil bacteria, *ACS Omega*, 2020, **5**, 7861-7876, doi: 10.1021/acsomega.9b04084.
[29] B. Lallo da Silva, M. P. Abuçafy, E. Berbel Manaia, J. A. Oshiro Jr, B. G. Chiari-Andréo, R. C. R. Pietro, L. A. Chiavacci, Relationship between structure and antimicrobial activity of zinc oxide nanoparticles: an overview, *International Journal of Nanomedicine*, 2019, **14**, 9395-9410, doi: 10.2147/ijn.s216204.
[30] J. Jiang, J. Pi, J. Cai, The advancing of zinc oxide nanoparticles for biomedical applications, *Bioinorganic Chemistry and Applications*, 2018, **2018**, 1062562, doi: 10.1155/2018/1062562.
[31] F. Leone, R. Cataldo, S. S. Y. Mohamed, L. Manna, M. Banchero, S. Ronchetti, N. Mandras, V. Tullio, R. Cavalli, B. Onida, Nanostructured ZnO as multifunctional carrier for a green antibacterial drug delivery system-a feasibility study, *Nanomaterials*, 2019, **9**, 407, doi: 10.3390/nano9030407.
[32] Y.-H. Hsueh, W.-J. Ke, C.-T. Hsieh, K.-S. Lin, D.-Y. Tzou, C.-L. Chiang, ZnO nanoparticles affect bacillus subtilis cell growth and biofilm formation, *PLoS One*, 2015, **10**, e0128457, doi: 10.1371/journal.pone.0128457.
[33] M. S. Holden, J. Black, A. Lewis, M.-C. Boutrin, E. Walemba, T. S. Sabir, D. S. Boskovic, A. Wilson, H. M. Fletcher, C. C. Perry, Antibacterial activity of partially oxidized Ag/Au nanoparticles against the oral pathogen Porphyromonas gingivalis W83, *Journal of Nanomaterials*, 2016, **2016**, 9605906, doi: 10.1155/2016/9605906.
[34] M. M. Mohamed, S. A. Fouad, H. A. Elshoky, G. M. Mohammed, T. A. Salaheldin, Antibacterial effect of gold nanoparticles against Corynebacterium pseudotuberculosis, *International Journal of Veterinary Science and Medicine*, 2017, **5**, 23-29, doi: 10.1016/j.ijvsm.2017.02.003.
[35] A. C. Martínez-Torres, H. Y. Lorenzo-Anota, M. G. García-Juárez, D. G. Zarate-Triviño, C. Rodríguez-Padilla, Chitosan gold nanoparticles induce different ROS-dependent cell death modalities in leukemic cells, *International Journal of Nanomedicine*, 2019, **14**, 7173-7190, doi: 10.2147/IJN.S221021.
[36] R. A. Murcia, S. M. Leal, M. V. Roa, E. Nagles, A. Muñoz-Castro, J. J. Hurtado, Development of antibacterial and antifungal triazole chromium(III) and cobalt(II) complexes: synthesis and biological activity evaluations, *Molecules*, 2018, **23**, 2013, doi: 10.3390/molecules23082013.
[37] D. Fonseca, S. M. Leal-Pinto, M. V. Roa-Cordero, J. D. Vargas, E. M. Moreno-Moreno, M. A. Macías, L. Suescun, Á. Muñoz-Castro, J. J. Hurtado, Inhibition of C. albicans dimorphic switch by cobalt(II) complexes with ligands derived from pyrazoles and dinitrobenzoate: synthesis, characterization and biological activity, *International Journal of Molecular Sciences*, 2019, **20**, 3237, doi: 10.3390/ijms20133237.
[38] M. Swierczewska, S. Lee, X. Chen, The design and application of fluorophore-gold nanoparticle activatable probes, *Physical Chemistry Chemical Physics*, 2011, **13**, 9929-9941, doi: 10.1039/c0cp02967j.
[39] A. Sirelkhatim, S. Mahmud, A. Seeni, N. H. M. Kaus, L. C. Ann, S. K. M. Bakhori, H. Hasan, D. Mohamad, Review on zinc oxide nanoparticles: antibacterial activity and toxicity mechanism, *Nano-Micro Letters*, 2015, **7**, 219-242, doi: 10.1007/s40820-015-0040-x.
[40] R. Singh, S. Cheng, S. Singh, Oxidative stress-mediated

 © Engineered Science Publisher LLC 2022

genotoxic effect of zinc oxide nanoparticles on Deinococcus radiodurans, *3 Biotech*, 2020, **10**, 66, doi: 10.1007/s13205-020-2054-4.
[41] K. S. Siddiqi, A. U. Rahman, Tajuddin, A. Husen, Properties of zinc oxide nanoparticles and their activity against microbes, *Nanoscale Research Letters*, 2018, **13**, 141, doi: 10.1186/s11671-018-2532-3.
[42] M. Nita, A. Grzybowski, The role of the reactive oxygen species and oxidative stress in the pathomechanism of the age-related ocular diseases and other pathologies of the anterior and posterior eye segments in adults, *Oxidative Medicine and Cellular Longevity*, 2016, **2016**, 3164734, doi: 10.1155/2016/3164734.
[43] M. Arakha, M. Saleem, B. C. Mallick, S. Jha, The effects of interfacial potential on antimicrobial propensity of ZnO nanoparticle, *Scientific Reports*, 2015, **5**, 9578, doi: 10.1038/srep09578.
[44] S. Khan, A. A. Ansari, A. A. Khan, R. Ahmad, O. Al-Obaid, W. Al-Kattan, In vitro evaluation of anticancer and antibacterial activities of cobalt oxide nanoparticles, *Journal of Biological Inorganic Chemistry*, 2015, **20**, 1319-1326, doi: 10.1007/s00775-015-1310-2.
[45] S. Chowdhury, Z. Wu, A. Jaquins-Gerstl, S. Liu, A. Dembska, B. A. Armitage, R. Jin, L. A. Peteanu, Wavelength dependence of the fluorescence quenching efficiency of nearby dyes by gold nanoclusters and nanoparticles: the roles of spectral overlap and particle size, *The Journal of Physical Chemistry C Nanomater. Interfaces*, 2011, **115**, 20105-20112, doi: 10.1021/jp204836w.
[46] B. M. Shenoy, G. Hegde, D. Roy Mahapatra, Field enhancement in microfluidic semiconductor nanowire array, *Biomicrofluidics*, 2020, **14**, 064102, doi: 10.1063/5.0028899.
[47] J. Xu, J. Yang, A. Nyga, M. Ehteramyan, A. Moraga, Y. Wu, L. Zeng, M. M. Knight, J. C. Shelton, Cobalt (II) ions and nanoparticles induce macrophage retention by ROS-mediated down-regulation of RhoA expression, *Acta Biomaterialia*, 2018, **72**, 434-446, doi: 10.1016/j.actbio.2018.03.054.
[48] H. Moradpoor, M. Safaei, F. Rezaei, A. Golshah, L. Jamshidy, R. Hatam, R. S. Abdullah, Optimisation of cobalt oxide nanoparticles synthesis as bactericidal agents, *Open Access Macedonian Journal of Medical Sciences*, 2019, **7**, 2757-2762, doi: 10.3889/oamjms.2019.747.
[49] R. Wan, Y. Mo, Z. Zhang, M. Jiang, S. Tang, Q. Zhang, Cobalt nanoparticles induce lung injury, DNA damage and mutations in mice, *Particle and Fibre Toxicology*, 2017, **14**, 38, doi: 10.1186/s12989-017-0219-z.
[50] J. M. Grim, M. C. Semones, D. E. Kuhn, T. Kriska, A. Keszler, E. L. Crockett, Products of lipid peroxidation, but not membrane susceptibility to oxidative damage, are conserved in skeletal muscle following temperature acclimation, *American Journal of Physiology - Regulatory Integrative and Comparative Physiology*, 2015, **308**, R439-R448, doi: 10.1152/ajpregu.00559.2013.
[51] J. M. Byrne, V. S. Coker, S. Moise, P. L. Wincott, D. J. Vaughan, F. Tuna, E. Arenholz, G. van der Laan, R. A. Pattrick, J. R. Lloyd, N. D. Telling, Controlled cobalt doping in biogenic magnetite nanoparticles, *Journal of the Royal Society Interface*, 2013, **10**, 20130134, doi: 10.1098/rsif.2013.0134.
[52] Y. A. Syed Khadar, A. Balamurugan, V. P. Devarajan, R. Subramanian, S. Dinesh Kumar, Synthesis, characterization and antibacterial activity of cobalt doped cerium oxide (CeO_2: Co) nanoparticles by using hydrothermal method, *Journal of Materials Research and Technology*, 2019, **8**, 267-274, doi: 10.1016/j.jmrt.2017.12.005.
[53] M. Altunbek, G. Kuku, M. Culha, Gold nanoparticles in single-cell analysis for surface enhanced Raman scattering, *Molecules*, 2016, **21**, 1617, doi: 10.3390/molecules21121617.
[54] K. Hamasha, Q. I. Mohaidat, R. A. Putnam, R. C. Woodman, S. Palchaudhuri, S. J. Rehse, Sensitive and specific discrimination of pathogenic and nonpathogenic Escherichia coli using Raman spectroscopy-a comparison of two multivariate analysis techniques, *Biomedical Optics Express*, 2013, **4**, 481-489, doi: 10.1364/BOE.4.000481.
[55] T. Ming, L. Zhao, Z. Yang, H. Chen, L. Sun, J. Wang, C. Yan, Strong polarization dependence of plasmon-enhanced fluorescence on single gold nanorods, *Nano Letters*, 2009, **9**, 3896-3903, doi: 10.1021/nl902095q.
[56] A. Samavati, M. K. Mustafa, A. F. Ismail, M. H. D. Othman, M. A. Rahman, Copper-substituted cobalt ferrite nanoparticles: structural, optical and antibacterial properties, *Materials Express*, 2016, **6**, 473-482, doi: 10.1166/mex.2016.1338.
[57] M. Sivachidambaram, J. J. Vijaya, K. Kaviyarasu, L. J. Kennedy, H. A. Al-Lohedan, R. Jothi Ramalingam, A novel synthesis protocol for Co_3O_4 nanocatalysts and their catalytic applications, *RSC Advances*, 2017, **7**, 38861-38870, doi: 10.1039/C7RA06996K.

Publisher's Note: Engineered Science Publisher remains neutral with regard to jurisdictional claims in published maps and institutional affiliations.

© Engineered Science Publisher LLC 2022